JTTEE5 7:219-228

PEER REVIEWED

Surface Roughness of Thermal Spray Coatings Made with Off-Normal Spray Angles

M.P. Kanouff, R.A. Neiser, Jr., and T.J. Roemer

(Submitted 20 October 1997; in revised form 9 March 1998)

The formation of a thermal spray coating using an off-normal direction angle for the spray has been analyzed to identify the causes of the large surface roughness of the coating. In the analysis, the string method was used for modeling the formation of the coating. The method uses a string of equally spaced node points to define the shape of the coating surface and to track the change in this shape as the thermal spray mass is deposited. The method allows for the calculation of arbitrary shapes for the coating surface that may be very complex. The model simulates the stochastic deposition of a large number of thermal spray droplets. Experiments were carried out to obtain the data used in the model for the mass flux distribution on the target surface. The data show that when the thermal spray mass impinges on the target surface a large fraction of it, called overspray, splashes off the target and is redeposited with a small direction angle. This component of the deposited mass results in a large coating roughness.

Keywords coating, coating formation simulation, high velocity oxygen fuel (HVOF), modeling, off-normal spray angle, over-spray, surface roughness, thermal spray

1. Introduction

Thermal spraying refers to a family of processes used to apply coatings on surfaces for providing enhanced protection from wear, corrosion, or thermal damage. In a cooperative research and development agreement (CRADA), General Motors and Sandia National Laboratories developed the high-velocity oxygen-fuel (HVOF) thermal spray process to apply a wear-resistant coating to the surfaces of aluminum engine cylinder bores (Ref 1). Figure 1 shows a schematic of the process hardware. Fuel (methane), oxygen, and air are supplied to the HVOF gun, where the fuel and oxygen react in a chamber called an air cap near the exit of the gun (Ref 2). The combustion process creates high-gas temperatures and pressures in the air cap. The coating material, steel, is fed into the gun in the form of wire, which is melted by the high gas temperatures. The high gas pressure in the air cap and nozzle construction accelerates the gas to high velocities. The gas flows over the wire and strips the molten steel off of it (Ref 3). The gas velocity atomizes the molten steel, that is, breaks it up into small droplets, which are accelerated and transported to the target surface where they are deposited. As illustrated in Fig. 1, the steel spray exits the gun and impinges on the surface of the cylinder bore with an off-normal angle. The HVOF gun rotates rapidly and strokes vertically along the axis of the cylinder bore to attain uniform deposition of the steel. The surface of the cylinder bore is roughened before coating to promote good bonding with the thermal sprayed coating.

M. P. Kanouff, Mechanics and Simulation of Manufacturing Processes Department, Sandia National Laboratories, Livermore, CA 94550; and **R. A. Neiser, Jr.** and **T. J. Roemer,** Direct Fabrication Department, Sandia National Laboratories, Albuquerque, NM 87185. Contact e-mail: kanouff@sandia.gov.

When the droplets strike the cylinder surface, they deform into small flat disk-shaped "splats." The heat in the splat rapidly conducts into the massive cylinder wall, and the splat solidifies. The solidification process occurs over a period of microseconds (Ref 4), and each splat is well solidified before another droplet is deposited on top of it.

One defect resulting from the spray process is that the coating has a very rough surface. A smooth surface is required because the engine piston rings must slide upon this surface and maintain a good seal between the cylinder bore surface and ring to contain the high-pressure gases created during engine operation. Consequently, a machining operation must be added to the overall production procedure to obtain the smooth coating surface. This increases the time and cost of the production procedure. Moreover, machining the coating is difficult due to the hardness of the material, which results in short lifetimes for the machine tools and increases the time and cost of the machining operation.

Experimental studies of roughness on the surfaces of thermally sprayed coatings have been done for sprays that are perpendicular to the substrate. Steeper et al. (Ref 5) used the twin-wire arc thermal spray process, and they studied the effects of the material feed rate, the spraying distance, and the gun traverse rate. Matsubara et al. (Ref 6) used the HVOF process, and they studied the effects of the roughness of the substrate and the coating thickness. Hasui et al. (Ref 7) used the plasma jet and oxyacetylene flame spray processes, and they studied the effects of the coating thickness. All of these studies showed that the surface roughness of the coating is small for sprays that are perpendicular to the substrate and that the effect of the process parameters is small. Hasui et al. (Ref 7) also studied the effect of the spray angle and showed that this parameter had a large effect on the coating roughness, where it increased as the spray angle decreased. Also, for a spray angle of 45° they showed that the coating roughness increased with the coating thickness. Smith et al. (Ref 8) also showed that the coating surface roughness is larger for nonperpendicular spray angles than for perpendicular spray angles.

Numerical models have been developed that predict the roughness of thermal spray coatings, although this was not their primary purpose. Cirolini, Harding, and Jacucci (Ref 9) studied the formation of a plasma sprayed thermal barrier coating for the purpose of calculating the porosity in the coating. Their results showed that the roughness of the coating surface was larger than the preroughness of the substrate. They did not investigate the effect of process parameters on the coating roughness. Knotek et al. (Ref 10) modeled the formation of a chromium coating as applied by a HVOF process with powder feedstock. Their results also showed that the roughness on the coating surface was larger than the roughness of the substrate, although they did not emphasize this aspect of their results. Both of these studies assumed the spray direction was perpendicular to the substrate.

There appears to be little work done to identify the causes of surface roughness on thermal spray coatings for nonperpendicular spray angles. This work therefore approaches the problem by developing a mathematical model for the formation of a thermal spray coating. An experiment was done to study some of the characteristics needed for modeling the thermal spray mass flux on a substrate for a nonperpendicular spray angle.

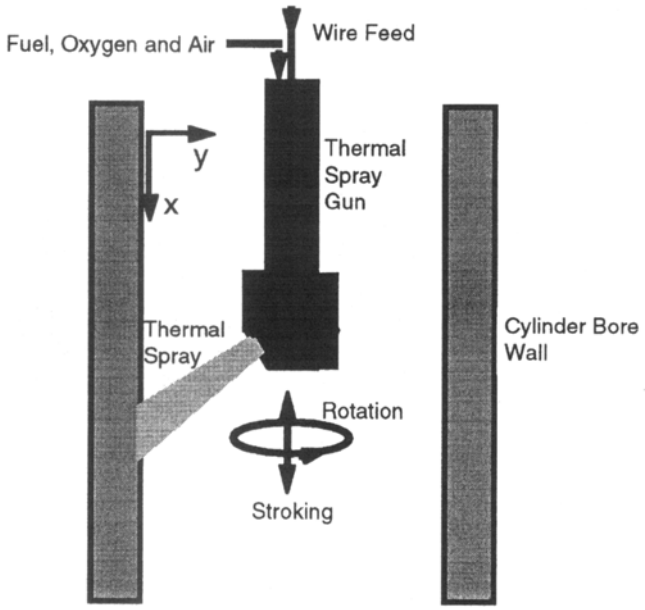

Fig. 1 HVOF process for coating engine cylinder bores

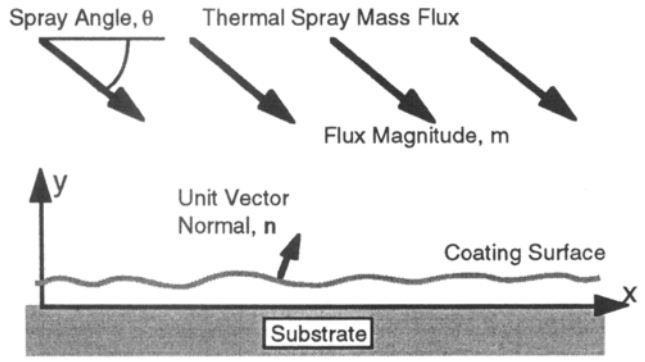

Fig. 2 Mass flux and coating profile

2. Mathematical Model of the Coating Formation

A model for the formation of a thermal spray coating was developed for calculating the shape and roughness of the coating surface. The model assumes the process is two-dimensional, in the x-y coordinate plane as shown in Fig. 1. The x-coordinate is parallel to the substrate surface (parallel to the axis of the cylinder bore), and the y-coordinate is normal to the substrate surface. The effects of surface curvature in the azimuthal direction of the cylinder bore are ignored, which is valid for coating thicknesses that are small compared to the radius of the cylinder bore. Only a small fraction of the axial length of the cylinder bore is modeled. This should be a good assumption as long as the length of cylinder bore included in the model is large compared to the coating thickness. The characteristics of the thermal spray mass flux are inputs to the model that were determined with the help of an experiment.

Nomenclature

D	Droplet size, μm
D_S	Droplet size in the over-spray, μm
f	Fraction of a splat located "upstream" of the droplet impact point
g	Rate of accumulation of mass on the coating surface, $gs^{-1}\,\mu m^{-2}$
L	Length of a splat, μm
$\mathbf{m}$	Thermal spray mass flux vector, $gs^{-1}\,\mu m^{-2}$
m	Thermal spray mass flux magnitude, $gs^{-1}\,\mu m^{-2}$
$\mathbf{n}$	Unit vector locally perpendicular to the coating surface
R_a	Roughness variable quantifying the dimension of the surface roughness elements perpendicular to the substrate, μm
$\mathbf{r}$	Position vector for a point on the coating surface, μm
S_m	Roughness variable quantifying the dimension of the surface roughness elements parallel to the substrate, μm
T	Thickness of a splat, μm
t	Time, s
W	Width of a splat, μm
w_i	Fraction of the thermal spray mass deposited in mass flux zone, i
y_m	Coating thickness, μm
β	Local impact angle of a droplet on the coating surface, degrees
χ	x-component of $\mathbf{n}$
δ	Time interval between droplet impacts, s
γ	y-component of $\mathbf{n}$
θ	Thermal spray direction angle, degrees
ρ	Density of the thermal spray material, $g\,\mu m^{-3}$
ξ	Spread coefficient for a perpendicular droplet impact
ξ′	Spread coefficient for a nonperpendicular droplet impact

Subscripts

b	Value for the coating surface segment, b
i	Value for the mass flux zone, i
k	Value for the node point, k

The rate of movement of a point on the coating surface is described by:

$$\frac{d\mathbf{r}}{dt} = \frac{g\mathbf{n}}{\rho} \quad \text{(Eq 1)}$$

where $\mathbf{r}$ is a position vector for the point ($\mathbf{r} = x\mathbf{i} + y\mathbf{j}$), which specifies its x and y coordinates, g is the rate at which the thermal spray mass accumulates per unit area of the surface, ρ is the density of the sprayed material, and $\mathbf{n}$ is the unit vector (dimensionless) locally normal to the coating surface (see Fig. 2). Equation 1 states that a point on the coating surface moves in the direction of $\mathbf{n}$. The quantity g depends on the thermal spray mass flux characteristics, the degree of spreading that a droplet undergoes when it impacts on the surface, and the shading that may take place when a part of the coating surface shades another part of the surface thereby preventing the direct impact of thermal spray droplets on that portion of the surface. The thermal spray mass flux vector, $\mathbf{m}$, is characterized by its magnitude, m, with units of mass per unit time per unit area, and its direction described in terms of the direction angle, θ, as defined in Fig. 2. In addition, the droplets in the thermal spray have a diameter, D. When g is determined and Eq 1 is solved for each and every point on the coating surface, a complete description of the evolution of the shape and position of the surface is obtained. An experiment was done to determine the distributions for m, θ, and D along the target surface, as described in the next section.

The thermal spray is assumed to consist of a large number of droplets that are randomly distributed within the spray. This is described in the model by dividing the target surface into a large number of small segments. The values of m, θ, D, and the segment length, l_b, are used in Eq 2 to determine the average time interval between droplet impacts on each segment. A random number generator is used to obtain random variations about this average time interval that are then used for the time interval between a specific pair of droplet impacts on a segment of the target surface.

$$\delta t = \frac{\pi D^3 \rho}{6 m l_b \sin\theta} \quad \text{(Eq 2)}$$

2.1 Shading

When large roughness elements develop on the coating surface, portions of the coating surface downstream of the roughness elements can be shaded from the thermal spray mass flux, as illustrated in Fig. 3. This can have large effects on the subsequent development of the shape of the coating surface. The model identifies the regions on the coating surface that are shaded from the thermal spray mass flux.

2.2 Droplet Spreading

When a thermal spray droplet impacts on the target surface it spreads out into a splat, which, for a perpendicular impact on a smooth surface, yields the shape of a flat circular disk. Perpendicular impacts on a rough surface often have "starlike" shapes (Ref 8). Dykhuizen (Ref 11) reviews the impact phenomena of thermal spray droplets. The extent of spreading of a droplet is described in terms of a spread coefficient, ξ, defined as the ratio of the diameter of the splat divided by the diameter of the droplet. Analyses of the spreading of a droplet during its impact with the target surface (Ref 12, 13) have shown that the spread coefficient depends on the Reynolds number of the droplet.

Experimental measurements of ξ for thermal spray droplets have been made and show much experimental scatter. Madejski (Ref 12) measured $5 < \xi < 6$ for the impact of plasma sprayed alumina droplets on (presumably) smooth surfaces. Fantassi et al. (Ref 14) measured $1 < \xi < 6$ and Bianchi et al. (Ref 15) measured $\xi = 5$ for the impact of plasma sprayed zirconia droplets on smooth surfaces. Moreau, Gougeon, and Lamontagne (Ref 16) studied the effect of target surface roughness on ξ for plasma sprayed molybdenum droplets. They measured $7 < \xi < 10$ for smooth targets, $5 < \xi < 7$ for fine grit blasted targets ($R_a = 1$ μm), and $4 < \xi < 5$ for coarse grit blasted targets ($R_a = 7$ μm).

Impacts that are not perpendicular have also been studied experimentally by Hasui, Kitahara, and Fukushima (Ref 7), Madejski (Ref 12), and Montavon et al. (Ref 17). In general, nonperpendicular impacts result in an elongation of the splat in the direction of the component of the droplet velocity parallel to the target, such that the splat has more of an oval shape. The length, L, of the splat shapes (which is different from the width of a splat for nonperpendicular impacts) obtained by Madejski (Ref 12) on smooth surfaces were measured, and the results are presented in Fig. 4 in terms of a modified spread coefficient defined as $\xi' = L/D$. Figure 4 shows ξ'/ξ as a function of the impact

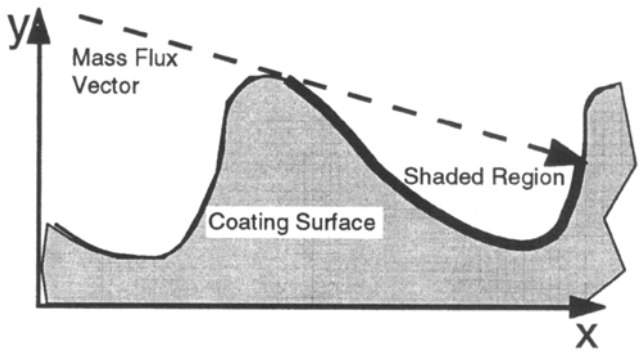

Fig. 3 Regions on the coating surface that are either shaded or exposed to the thermal spray mass flux

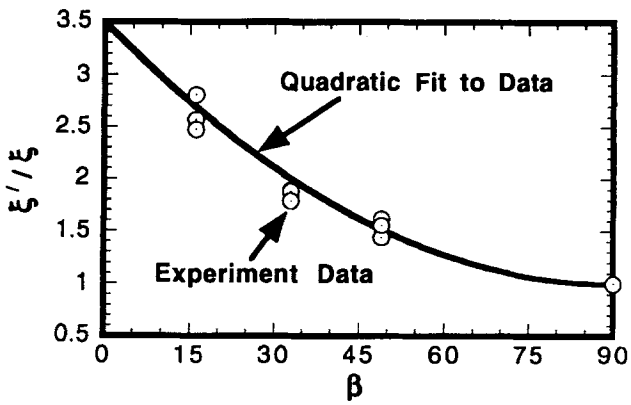

Fig. 4 Data by Madejski (Ref 12) for the splat length as a function of impact angle

angle, where $\xi' = \xi$ for a perpendicular impact. A quadratic polynomial function of the impact angle, β ($\beta = 90°$ is perpendicular), provides a good approximation to the data as shown in Fig. 4:

$$\frac{\xi'}{\xi} = 3.5 - 0.0556\beta + 0.000309\beta^2 \quad \text{(Eq 3)}$$

It is assumed that when a droplet impacts on the target surface, it spreads out to form a splat with a length, L, a width, W, and a uniform thickness, T. Due to the nonperpendicular impact of the thermal spray jet in the thermal spray process studied here, there is a predominance of nonperpendicular droplet impacts. Hence, the spread coefficient is computed using Eq 3 to account for the elongation effect that nonperpendicular impacts have on the shape of the splats. A prescribed value of ξ corresponding to a perpendicular impact is used (typically values between 3 and 5) along with Eq 3 for ξ' to obtain the length of a splat using:

$$L = \xi' D \quad \text{(Eq 4)}$$

Here, the impact angle, β, is the local impact angle that depends not only on the direction angle, θ, of the spray, but also on the local inclination angle of the coating surface, as shown in Fig. 5.

It is assumed that the position of the splat relative to the droplet impact point depends on the impact angle, β. The appearance of the splats obtained by Madejski (Ref 12) created by nonperpendicular impact angles indicates that the splat length is not centered about the impact point, rather the position of the splat center is downstream of the impact point, that is, in the direction of the component of the droplet velocity parallel to the target surface. This is described in terms of the fraction of the splat, f, which lies upstream of the impact point, which is assumed to be a function of the local impact angle, β. Due to the absence of data for the relationship between f and β for a droplet impact, a simple linear relationship is used here for f as given in:

$$f = \frac{\beta}{180°} \quad \text{(Eq 5)}$$

Equation 5 gives the result, $f = 1/2$, for $\beta = 90$; that is, the splat center is located at the impact point for a perpendicular impact, as it should based on symmetry considerations. It also gives the result that the splat is located entirely downstream of the impact point for a glancing impact, $\beta = 0$.

The splat is assumed to have a uniform thickness. The splat width, W, is assumed to equal the splat size for a normal impact, $W = \xi D$. In general, there is more than one droplet size included in the thermal spray mass flux distribution, so a direct application of this equation for W would lead to different splat widths. Because the model is two dimensional, it is desirable to give all splats the same width. This is done by basing W on the largest size used for the droplets regardless of the size of the droplets forming the splats.

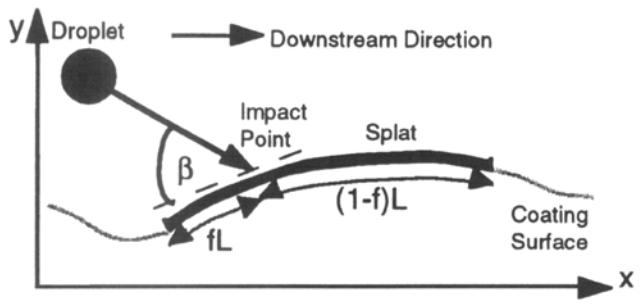

Fig. 5 Location of a splat relative to the droplet impact point on the coating surface

2.3 Initial Condition

The initial condition for the shape of the target surface is the shape of the preroughened substrate profile. Surface profile measurements of an actual preroughened surface are used in the model. These are obtained from a laser profilometer, which is used to scan the surface of a preroughened substrate. The shape of the surface is described in terms of the coordinates of a large number of equally spaced points.

2.4 Boundary Condition

Recall that only a portion of the actual coating is included in the simulations. This computed portion can be affected by portions of the coating surface not included in the model by the shading that they cause; that is, the portions of the surface not included in the model may cast shadows (and prevent the direct deposition of the thermal spray mass flux) on the computed portion of the coating surface. The computed portion of the coating surface can also be affected by droplet impacts that occur outside of the computed portion of the surface but spread out into splats such that mass is deposited on the computed portion of the surface. These effects are accounted for by using a periodic boundary condition where it is assumed that the computed surface repeats itself. Thus, a shadow cast by one end of the computed surface is assumed to fall on the other end. Similarly, the portion of a splat that moves off one end of the computed surface is assumed to move onto the other end of the computed surface.

2.5 Solution Methodology

A numerical procedure called the string method (Ref 18) is used to implement the analysis described previously. The surface of the coating is defined with a set of equally spaced node points. These node points track the position and shape of the coating surface as they change due to the deposition of the sprayed material. Equation 1 is discretized as:

$$\frac{\Delta \mathbf{r}_k}{\Delta t} = \frac{g_k \mathbf{n}_k}{\rho} \rightarrow \frac{\Delta x_k}{\Delta t}\mathbf{i} + \frac{\Delta y_k}{\Delta t}\mathbf{j} = \frac{g_k}{\rho}(\chi_k \mathbf{i} + \gamma_k \mathbf{j}) \quad \text{(Eq 6)}$$

where $\mathbf{i}$ and $\mathbf{j}$ are the unit vectors in the x and y directions, respectively, and χ_k and γ_k are the x and y components, respectively, for the unit vector locally normal to the coating surface, and the subscript, k, refers to a specific node. This equation can be split into its $\mathbf{i}$ and $\mathbf{j}$ components to obtain equations for the change in the x and y coordinates, Δx_k and Δy_k, respectively, which take place due to the mass deposition during the time step, Δt, for the node k. The components of the local normal unit vector at node k are computed using:

$$\chi_k = \frac{y_{k-1} - y_{k+1}}{|\mathbf{r}_{k+1} - \mathbf{r}_{k-1}|} \quad \text{(Eq7a)}$$

$$\gamma_k = \frac{x_{k+1} - x_{k-1}}{|\mathbf{r}_{k+1} - \mathbf{r}_{k-1}|} \quad \text{(Eq7b)}$$

Equation 6 is solved for each node using an explicit first-order method where current values of the nodal coordinates are used to determine the values for g_k, χ_k, and γ_k. At the beginning of each time step the nodes are equally spaced along the coating surface. The extent of shading is determined to identify the set of nodes exposed to the current mass flux. All droplet impact events are then identified along with their position. A droplet impact event occurs within a segment of the coating surface if $t < t_b + \delta t_b < t + \Delta t$, where t_b is the time of the last droplet impact in segment b, and δt_b is the next time interval between droplet impacts within segment b. The location of the impact is the exposed node at the center of the segment b.

After all droplet impact events are identified, droplet spreading is computed. For each droplet impact event, the local impact angle, β, is computed using Eq 8.

where $k-1$ and $k+1$ refer to the neighboring nodes as shown in Fig. 6.

$$\beta = \cos^{-1}(\sin\theta \cdot \chi_k - \cos\theta \cdot \gamma_k) \quad \text{(Eq 8)}$$

The length of the splat, L, is computed using Eq 3 and 4, the position of the splat relative to the impact point as described by f is computed using Eq 5, and the thickness of the splat, T, is computed as the volume of the droplet divided by L and the width of the splat, W. The quantity, $T/\Delta t$, is then added to g_k for all nodes, k, which are within the distance fL upstream of the impact point, and to all nodes, k, which are within the distance $(1-f)L$ downstream of the impact point. This is done for each droplet impact event. This gives the values for g_k. The coordinates of the node points are then incremented using :

$$x_k^{n+1} = x_k^n + g_k \cdot \chi_k \cdot \Delta t \quad \text{(Eq 9a)}$$

$$y_k^{n+1} = y_k^n + g_k \cdot \gamma_k \cdot \Delta t \quad \text{(Eq 9b)}$$

and time is incremented as $t^{n+1} = t^n + \Delta t$, where the superscripts, n and $n+1$, are used to denote old and new values, respectively.

In general, the process of incrementing the nodal coordinates results in a nonequal distribution of the node points along the coating surface. If the nonuniformity in the node spacing becomes large, this can result in the generation of erroneous results. Hence, the nodes are redistributed along the coating surface after every time step in order to maintain the uniform node spacing (typically the spacing is on the order of 3 μm).

This completes one time step, and at this point the calculations begin again for the next time step beginning with an update of the mass flux characteristics for the current time and an evaluation of the shading that occurs on the current shape of the coating surface.

3. Experimental Study of Thermal Spray Mass Flux Distribution

An important step in identifying the causes of the rough surfaces on the thermal spray coatings is to determine the characteristics of the thermal spray mass flux on the target surface. An experiment was carried out to determine these characteristics. Figure 7 shows a schematic of the experiment used to study the distribution of mass deposited on a flat plate by a thermal spray gun with an angled air cap. A Metco DJ thermal spray gun with an M2 air cap (Sulzer Metco, Westbury, NY) (Ref 2) was used to make a deposit on the plate where the plate was held parallel to the axis of the gun and at a distance from the gun corresponding to the radius of the engine cylinder bore. The gun did not stroke, and it did not rotate. After gun startup, the gun traversed across the plate (normal to the plane of Fig. 7) at 2.54 m/min (100 in./min). A total of 15 passes were used to make the deposit. A grit-blasted aluminum plate with dimensions 5.08 by 20.32 by 0.32 cm (2 by 8 by 0.125 in.) was used as the target.

Figure 8 shows an infrared video image of the thermal spray as it impinged the plate. The image of the main spray coming from the gun can be seen as a narrow, slightly diverging cone as it approaches the plate. It remains approximately straight; that is, there is not a lot of curvature in the image. The direction angle, θ, of the main spray is approximately 51°. The area over which the main spray appears to impact the target plate is approximately 15 mm long. Starting from the main spray impact zone, a very bright elongated image parallel to the plate can be seen that extends approximately 5 mm above the plate and is

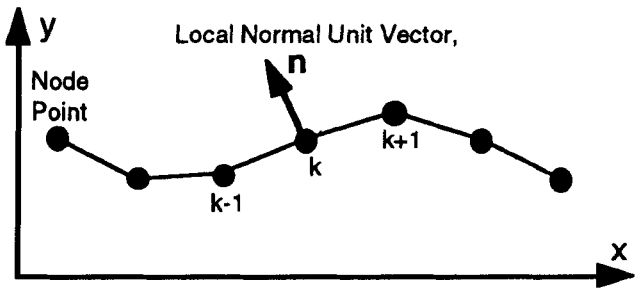

Fig. 6 Node point distribution along the coating surface

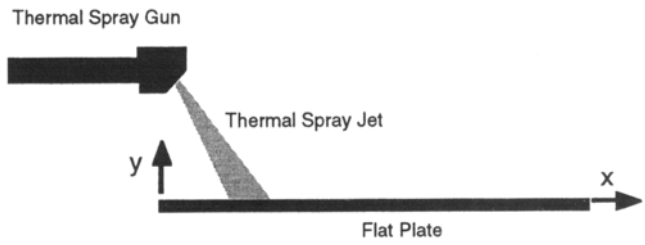

Fig. 7 Experimental arrangement used to make a thermal spray deposit on a flat plate. The thermal spray gun traversed across the plate (normal to the plane of the figure).

70 mm long. The material emitting this bright image appears to be the by-product of the thermal spray droplets splashing as they impact on the plate, where the splash product, called overspray, is ejected off the plate surface and is swept downstream parallel to the plate (positive x-direction shown in Fig. 7) by the gas flow. The location and length of this bright image corresponds to the location and length of the mass deposit that was later found on the plate. Thus, the thermal spray droplets appear to splash due to their impact on the target and the splashed product is redeposited on the target over an area that is several centimeters long.

The plate and deposit were cut and polished to create a metallurgical sample of the cross section (in the plane of Fig. 7) of the deposit, which was then photographed. The photograph of the deposit cross section was digitized, giving geometric definition of its boundaries and is shown in Fig. 9. The portion of the deposit near the impact zone of the main spray jet, the main deposit, was relatively thick with small roughness elements on it. This portion of the deposit had buckled and separated from the plate due to the thermal stresses created by the transfer of a large amount of heat in the thermal spray to the plate and deposit. The portion of the mass deposited away from the main spray impact zone, the overspray deposit, was in the form of isolated columns of material that were separated by large spaces. This structure is due to the deposition of material with a very small direction angle, as discussed below. A micrograph of the portion of the deposit composed of columns (within zones 4 and 5) is shown in Fig. 10.

The data shown in Fig. 8 and 9 were used to help estimate the distributions of m, θ, and D along the plate. The deposit cross section shown in Fig. 9 was divided into six zones that could be characterized as locally uniform in terms of the shape and thickness of the deposit. One of the zones, 2, covers the main deposit and the other five zones in combination cover the overspray deposit. The fraction of the deposit, w_i, located within each zone, i, based on the cross-sectional areas of the deposit are shown in Table 1. The mass flux per unit width of plate, m_i, for each zone i is given by:

$$m_i = \frac{M_g w_i}{S_i \sin \theta_i} \qquad \text{(Eq 10)}$$

where M_g is the material feed rate to the thermal spray gun, w_i is the fraction of the deposit located within the zone, S_i is the length of the zone, and θ_i is the direction angle of the spray in the zone. As discussed previously, the direction angle for the main spray (zone 2) is 51°, and the droplet size for the main spray deposit is 40 μm which is based on the measurements by Neiser (Ref 19). Calculations were carried out to estimate the values of θ_i and D_i for the remaining zones which span the over-spray deposit. A value of 5 was used for ξ (the spread coefficient for perpendicular droplet impacts used in Eq 3) in these calculations, which are described in the Appendix to this article. These results for the values of w_i, θ_i, and D_i are summarized in Table 1. These results show that most of the mass is deposited in the main spray impact zone (zone 2) where θ and D are relatively large and that a significant amount (23%) of the mass is deposited in the overspray

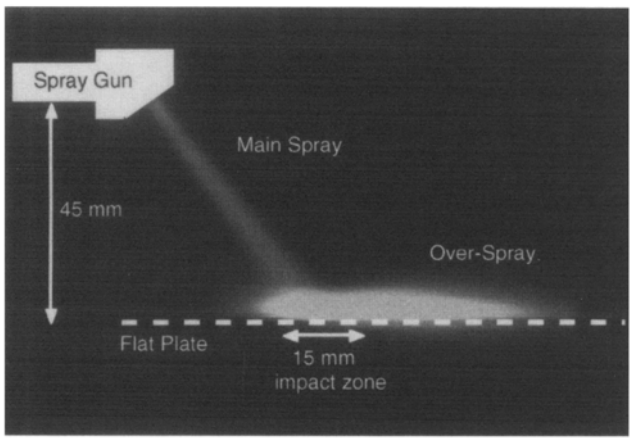

Fig. 8 Infrared image of the HVOF thermal spray impinging on a flat plate

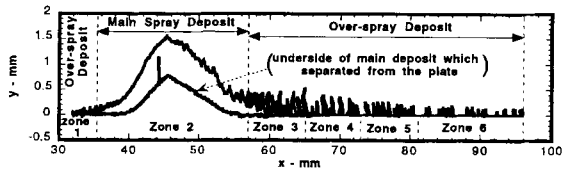

Fig. 9 Digitized data for the shape of the deposit cross section obtained from the experiment

Table 1 Distributions for the deposited mass, direction angle, and droplet size in a HVOF thermal spray jet impinging on a flat plate

Zone No.	Description	Thermal spray direction angle (θ), degrees	Droplet size (D), μm	Deposited mass (w), %
1	Overspray	178	5	1
2	Main spray	51	40	76.6
3	Overspray	7.5	15	14.4
4	Overspray	5	15	4
5	Overspray	3	10	2
6	Overspray	2	5	2

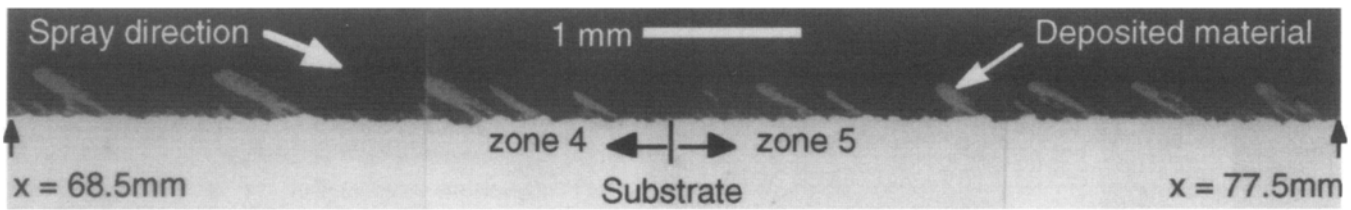

Fig. 10 Micrograph of the portion of the deposit composed of columns spanning the rear half of zone 4 and the forward half of zone 5

zones (zones 1 and 3 to 6) where D is small and the direction angles are very shallow.

4. Results

The results for the coating roughness are presented in terms of the roughness variables, R_a and S_m, which provide measures for the average height and spacing, respectively, of the roughness elements that form on the surface of the coating. R_a is defined as:

$$R_a = \frac{1}{\Delta X_t} \int_0^{\Delta X_t} |y - y_m| dx \qquad \text{(Eq 11)}$$

where ΔX_t is the length of the model target, and y_m is the average height of the coating surface, also called the coating thickness. S_m is the average distance between the peaks of the roughness elements on the coating surface as measured parallel to the x-axis and is given by:

$$S_m = \frac{\Delta X_t}{\text{Number of peaks}} \qquad \text{(Eq 12)}$$

As shown in Fig. 11, the peak of a roughness element is defined as the highest point on the coating surface with a height, y, that is above the elevation given by $y_m + 0.5*R_a$ and is separated from other peaks by points on the coating surface with heights that are below the elevation given by $y_m - 0.5*R_a$, called valleys. Note that this is the definition used here, and that other definitions for S_m are possible (Ref 20).

The calculations were tested for convergence with respect to the numerical parameters. The effect of reducing by a factor of two the number of node points used to define the coating surface relative to the number used in most of the calculations (8000) resulted in a maximum difference in R_a of 4%. The effect of reducing the time step by a factor of two used to integrate Eq 1 was to change the results by 2%. The effect of the random number sequence used for determining the droplet impact times was less than 1%.

A uniform coating thickness is obtained on the cylinder bore by moving the thermal spray gun with constant speed along the axis of the bore while the bore is held stationary. Alternatively, the bore may be considered to move while the gun remains stationary. This is simulated in the model by specifying that the small portion of the target surface included in the model moves with constant speed back and forth through the thermal spray mass zones described in Table 1. The number of cycles used for the movement of the target relative to the gun was 55.

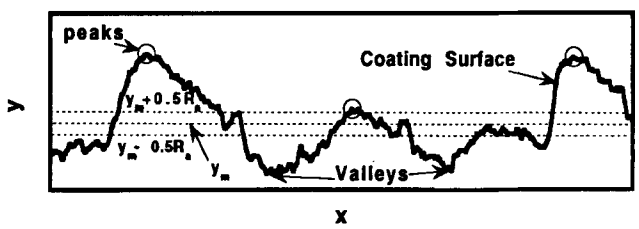

Fig. 11 Coating surface and arrangement of peaks and valleys

4.1 Comparison with Experimental Data

In order to provide data for comparison with the results from the calculations, a set of coatings were made with various thicknesses on cylinders with geometries similar to engine cylinder bores. A laser profilometer was used to measure the profiles of the coatings along lines 25 mm (1 in.) in length (parallel to the cylinder axis) at several locations on each coating. The roughness characteristics of the coatings were determined from the profile data.

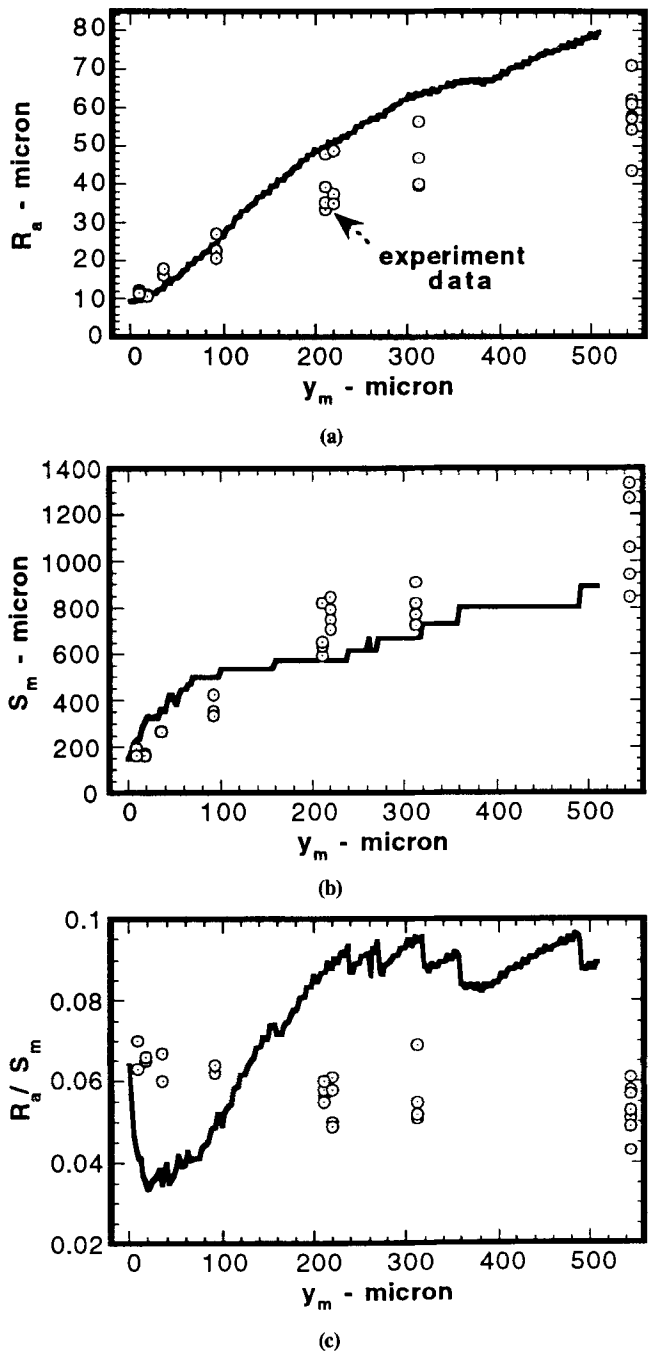

Fig. 12 Comparison of calculated and measured results for the coating roughness as a function of the coating thickness, y_m. (a) R_a. (b) S_m. (c) R_a/S_m

Figure 12 shows the measured and calculated results for R_a, S_m, and R_a/S_m. Both the measured and calculated results show that both R_a and S_m increase monotonically throughout the process. However, the calculated results overpredict R_a and underpredict (on average) S_m. Interestingly, the ratio R_a/S_m shown in Fig. 12(c), which may be interpreted as an average value for the roughness element aspect ratio, attains a near-steady value in both the calculated and measured results. However, the near-steady value for R_a/S_m is 0.06 for the experimental results, while it is 0.09 for the calculated results.

The results from the calculations for the shape of the coating surface are compared to experimental data in Fig. 13. A laser profilometer was used to measure this profile, which scans the coating surface vertically from above; consequently, it is not capable of resolving "overhanging" features of the roughness elements, as obtained in the calculations. Figure 14 shows a micrograph of one of the roughness elements in the coating that has this overhanging feature. Consistent with the comparison between calculated and measured results for R_a discussed above, the height of the roughness elements in the calculated results appear (Fig. 13) larger than in the measured results.

The reason for the disagreement between the calculated and measured results for roughness is unknown. It may be due to the different orientations used for the substrates with respect to gravity in the flat-plate experiment used to generate data for the mass flux distribution (see section 3) and the engine cylinder bore experiments used to generate data for the surface roughness (see section 4.1). Gravity may have a large effect on the trajectory of the overspray. In the flat-plate experiment it was perpendicular to the substrate, perhaps resulting in the deposition of a larger amount of overspray than that which occurred in the engine cylinder bore experiments where gravity was parallel to the substrate (i.e., the cylinder bore axis was vertical). Other possible sources for the discrepancy between the calculated and measured results include the assumption used in the calculations that the process is two dimensional in the x-y plane. This may neglect important out-of-plane thermal spray deposition angles that could result in the deposition of material between roughness elements, which would reduce the coating roughness. Also, the assumptions used for droplet spreading in the calculations may neglect important phenomena that could contribute to the disagreement.

4.2 Parameter Study

While the model overpredicts the coating surface roughness, its prediction for the sensitivity of the roughness to the input parameters may still be valid. Thus, the model was used

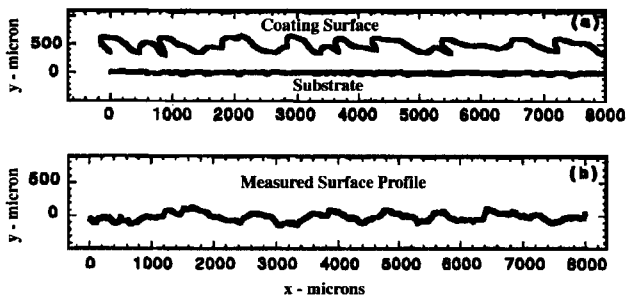

Fig. 13 The shape of the coating surface. (a) Calculated. (b) Measured

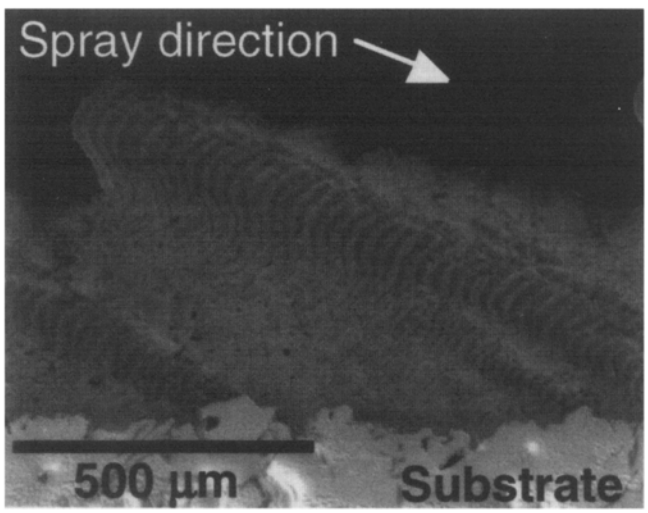

Fig. 14 Micrograph of a cross section of a roughness element in the coating, as viewed tangentially to the substrate. The direction of the thermal spray is toward the right.

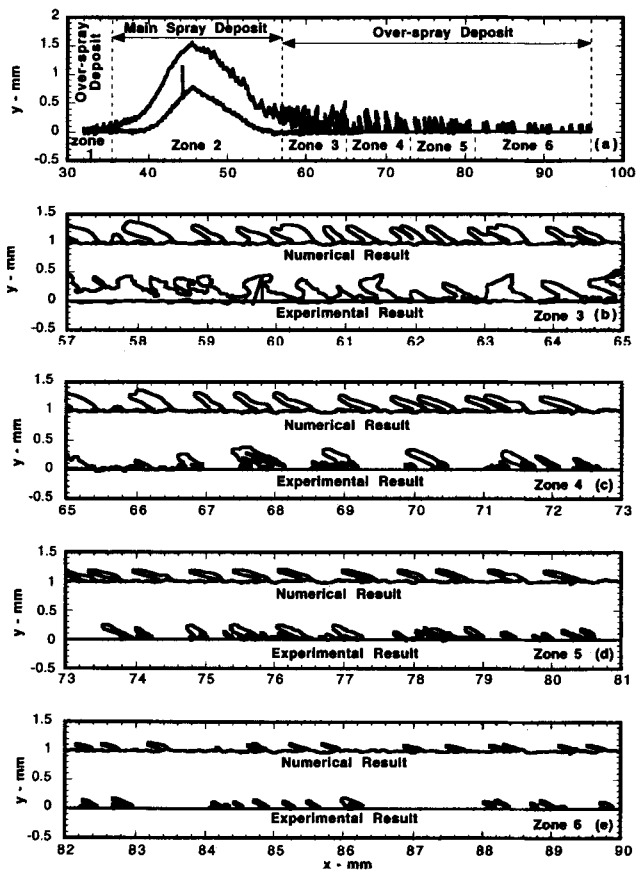

Fig. 15 Comparison of numerical and experimental results for the shape of the deposit formed on a flat plate. The digitized experimental data of the deposit cross section (a), and both numerical and experimental results for zone 3 (b), zone 4 (c), zone 5 (d), and zone 6 (e)

in a parameter study to predict the sensitivity of the coating surface roughness to the input parameters. The parameters considered were the preroughness on the substrate (prior to coating), the droplet size, the splash fraction (the fraction of the mass deposited by the overspay portion of the mass flux distribution), and the direction angle for the overspray. The model was used to vary these parameters independently, which is not possible with experimentation. The effects of changes in the parameters are expressed relative to the *baseline* case. The baseline case is characterized by the droplet sizes, mass deposit fractions, and direction angles presented in Table 1.

The effect of the preroughness on the substrate had very little effect on the coating roughness for coating thicknesses greater than 100 μm. Starting from a perfectly smooth substrate, calculated results for the coating roughness were observed to rapidly increase with coating thickness to values near those obtained for a preroughened substrate. Basically, it appears that the smooth coating surface is unstable, and it remains smooth only if there are no disturbances present, such as a preroughened substrate. Even the height changes created by the stochastic deposition of the droplets themselves are sufficient to destabilize the smooth surface on the coating.

In general, the coating roughness was found to decrease with decreasing droplet size, decreasing splash fraction and increasing direction angle of the overspray. The effects of changing these quantities from their baseline values by factors of two are shown in Table 2.

5. Conclusions

An analysis was done of the formation of surface roughness on thermal spray coatings applied with off-normal spray angles. An experiment was done to identify the characteristics of the thermal spray mass flux impinging on the substrate surface. The data from this experiment were combined with a model for the formation of the thermal spray coating to identify the causes of surface roughness. The model uses the string method where a string of equally spaced node points are used to define the shape of the coating surface and to track the changes in this shape as the thermal spray mass is deposited. This method allows for the calculation of arbitrary shapes for the coating surface that may be very complex.

An experiment was done where a thermal spray gun was used to make a deposit on a flat plate. An infrared image of the thermal spray jet impinging on the plate was captured. This image showed that the main spray jet impinges on the target surface at an angle of 51°. It also showed, in combination with the data for the shape and location of the deposit on the plate, that a large amount of splashing occurs when the thermal spray droplets impact on the target surface (at least 23%), and that the splashed material, called overspray, redeposits over large areas on the target surface. The coating formation model was used to analyze the structure of the redeposited overspray on the plate, which was composed of isolated columns with large spaces between them. Using a trial-and-error procedure, the calculations identified that the direction angle of the overspray on the plate was less than 8°.

The model was used to calculate the shape of coating surfaces resulting from the process used to coat engine cylinder bores. The primary causes of the large roughness was identified to be the large amount of overspray that redeposits on the substrate and the small direction angle of this overspray. A 50% reduction in the amount of overspray decreases the roughness by 42%, and a factor of two increase in the direction angle of the overspray decreases the roughness by 41%.

Table 2 The effect on coating roughness, R_a, of changing the values of quantities characterizing the thermal spray mass flux from their baseline values

Quantity	Change from baseline value	Effect on R_a
Droplet size	Reduced by factor of 2	18% decrease
Splash fraction	Reduced by factor of 2	42% decrease
Overspray direction angle	Increased by factor of 2	41% decrease

Acknowledgment

This work was funded through a Cooperative Research and Development Agreement between Sandia National Laboratories and the General Motors Corporation.

References

1. L. Byrnes and M. Kramer, Method and Apparatus for the Application of Thermal Spray Coatings Onto Aluminum Engine Cylinder Bores, *Thermal Spray Industrial Applications,* C.C. Berndt and S. Sampath, Ed., ASM International, 1994, p 39-42
2. B. Hassan, A.R. Lopez, and W.L. Oberkampf, Computational Analysis of a Three-Dimensional High-Velocity Oxygen-Fuel (HVOF) Thermal Spray Torch, *Thermal Spray Science and Technology,* C.C. Berndt and S. Sampath, Ed., ASM International, 1995, p 193-198
3. R.A. Neiser, J.E. Brockmann, T.J. O'Hern, R.C. Dykhuizen, M.F. Smith, T.J. Roemer, and R.E. Teets, Wire Melting and Droplet Atomization in a HVOF Jet, *Thermal Spray Science and Technology,* C.C. Berndt and S. Sampath, Ed., ASM International, 1995, p 99-104
4. J.H. Harding, P.A. Mulheran, S. Cirolini, M. Marchese, and G. Jacucci, Modeling the Deposition Process of Thermal Barrier Coatings, *J. Therm. Spray Technol.,* Vol 4, 1995, p 34-40
5. J. Steeper, G. Irons, W.R. Kratochvil, D.J. Varacalle, Jr., G.C. Wilson, R.W. Johnson, and W.L.Riggs (II), A Taguchi Experiment Design Study of Twin-Wire Electric Arc Sprayed Aluminum Coatings, *Themal Spray: International Advances in Coatings Technology,* C.C. Berndt, Ed., ASM International, 1992, p 427-432
6. Y. Matsubara and A. Tomiguchi, Surface Texture and Adhesive Strength of High Velocity Oxy-Fuel Sprayed Coatings for Rolls of Steel Mills, *Themal Spray: International Advances in Coatings Technology,* C.C. Berndt, Ed., ASM International, 1992, p 637-641
7. A. Hasui, S. Kitahara, and T. Fukushima, On Relation between Properties of Coating and Spraying Angle in Plasma Jet Spraying, *Trans. Nat. Res. Inst. Met.,* Vol 12 (No. 1), 1970, p 9-20
8. M.F. Smith, R.A. Neiser, and R.C. Dykhuizen, An Investigation of the Effects of Droplet Impact Angle in Thermal Spray Deposition, *Thermal Spray Industrial Applications,* C.C. Berndt and S. Sampath, Ed., ASM International, 1994, p 603-608
9. S. Cirolini, J.H. Harding, and G. Jacucci, Computer Simulation of Plasma-Sprayed Coatings. I. Coating Deposition Model, *Surf. Coat. Technol.,* Vol 48, 1991, p 137-145
10. O. Knotek, E. Lugscheider, P. Jokiel, U. Schnaut, and A. Wiemers, Chromium Coatings by HVOF Thermal Spraying: Simulation and Practical Results, *Thermal Spray Industrial Applications,* C.C. Berndt and S. Sampath, Ed., ASM International, 1994, p 179-184

11. R.C. Dykhuizen, Review of Impact and Solidification of Molten Thermal Spray Droplets, *J. Therm. Spray Technol.*, Vol 3 (No. 4), 1994, p 351-361
12. J. Madejski, Solidification of Droplets on a Cold Surface, *Int. J. Heat Mass Transfer*, Vol 19, 1976, p 1009-1013
13. H. Fukanuma, A Porosity Formation and Flattening Model of an Impinging Molten Particle in Thermal Spray Coatings, *J. Therm. Spray Technol.*, Vol 3 (No. 1), 1994, p 33-44
14. S. Fantassi, M. Vardelle, A. Vardelle, and P. Fauchais, Influence of the Velocity of Plasma Sprayed Particles on the Splat Formation, *Thermal Spray: Research, Design and Applications*, C.C. Berndt and T.F. Bernecki, Ed., ASM International, 1993, p 1-6
15. L. Bianchi, F. Blein, P. Lucchese, M. Vardelle, A. Vardelle, and P. Fauchais, Effect of Particle Velocity and Substrate Temperature on Alumina and Zirconia Splat Formation, *Thermal Spray Industrial Applications*, C.C. Berndt and S. Sampath, Ed., ASM International, 1994, p 569-574
16. C. Moreau, P. Gougeon, and M. Lamontagne, Influence of Substrate Preparation on the Flattening and Cooling of Plasma-Sprayed Particles, *J. Therm. Spray Technol.*, Vol 4 (No. 1), 1995, p 25-33
17. G. Montavon, C. Coddet, S. Sampath, H. Herman, and C.C. Berndt, Vacuum Plasma Spray Forming of Astroloy: An Investigation of Processing Parameters, *Thermal Spray Industrial Applications*, C.C. Berndt and S. Sampath, Ed., ASM International, 1994, p 469-475
18. R. Jewett, "A String Model Etching Algorithm," Memorandum No. UCB/ERL M79/68, SAMPLE Report No. SAMD-3, University of California, Berkeley, CA, 18 Oct 1979
19. R.A. Neiser, Private communication, Sandia National Labs, Albuquerque, NM, Jan 1996
20. M. Sander, *A Practical Guide to the Assessment of Surface Texture*, Fienprüf Perthen GmbH, Göttingen, 1991, p 15-81

Appendix: Calculations for the Thermal Spray Mass Flux Distributions

Calculations were done to determine the droplet size and direction angle of the spray in each of the over-spray deposit zones shown in Fig. 15(a). The droplet size and direction angle were assumed to be constant and locally uniform within each zone. A trial-and-error procedure was used to identify the values of these parameters, which are inputs to the model, that gave results for the shape of the deposit which compared with the results from the experiment. The results from the experiment for the shape of the deposit in the overspray zones showed that it was composed of isolated columns of material with large spaces in between. The calculated results also showed this structure for the deposit shape. The width of the columns and the distances between them were found to be sensitive to the droplet size and the direction angle used.

Figures 15(b) through (e) show the calculated results for the shape of the deposit in comparison to the experimental results for each overspray zone. The roughness of the preroughened substrate, in terms of R_a and S_m, used for the experiment was also used for the calculations, but the precise shape of the substrate profile used in the calculations was not the same as in the experiment, so a direct comparison between columns formed in the experiment cannot be made to those formed in the calculations. The comparison is good for the overall width of the columns and the distances between them.